Available online at www.sciencedirect.com
ScienceDirect
Optik 121 (2010) 1497–1506
Optik Optics
www.elsevier.de/ijleo

Acousto-optical spectrum analysis of ultra-high-frequency radio-wave analogue signals with an improved resolution exploiting the collinear acoustic wave heterodyning

Alexandre S. Shcherbakov[a], Alexey M. Bliznetsov[b,1], Abraham Luna Castellanos[a], Daniel Sanchez Lucero[a,*]

[a]*Department of Optics, National Institute for Astrophysics, Optics, and Electronics (INAOE), A.P. 51 y 216, Puebla, Pue. 72000, Mexico*
[b]*State Polytechnic University, Polytechnicheskaya St. 29, Saint-Petersburg 195251, Russia*

Received 28 October 2008; accepted 7 February 2009

Abstract

This article is devoted to the problem of improving the frequency resolution inherent in a parallel acousto-optical spectrum analysis via involving an additional nonlinear phenomenon into the data processing. In so doing, we examine possible application of the wave heterodyning to the real-time scale acousto-optical analysis of the frequency spectrum belonging to ultra-high-frequency radio-wave signals peculiar, for example, for radio-astronomy. The nonlinear process of wave heterodyning is realized through providing a co-directional collinear interaction of the longitudinal acoustic waves of finite amplitudes. This process, which is beforehand studied theoretically and investigated experimentally via the acousto-optical technique as well, allows us either to improve the frequency resolution of spectrum analysis at a given frequency range or to increase by a few times the current frequencies of radio-wave signals under processing. The first step along this way is connected with the experimental modeling of the acoustic wave heterodyning in solids via exploitation of the specific acousto-optical cell based on a liquid, which allows the simplest realization of a cell with the needed properties. Then, these theoretical and practical findings are used in our experimental studies aimed at creating a new type of acousto-optical cells, which are able to improve the resolution inherent in acousto-optical spectrum analyzer operating over ultra-high-frequency radio-wave signals. In particular, the possibility of upgrading the frequency resolution through the acoustic wave heterodyning is experimentally demonstrated using the cell made of lead molybdate crystal. The obtained results demonstrate practical efficiency of the novel approach presented.

Keywords: Acousto-optical spectrum analysis; Waves of the finite amplitude; Collinear wave heterodyning

1. Introduction

A major portion of modern developments in a high-speed and extremely precise optical data processing is currently connected with applying various nonlinear

*Corresponding author. Tel./fax: +52 222 247 2940.
E-mail addresses: alex@inaoep.mx (A.S. Shcherbakov), abliznetsov@mail.ru (A.M. Bliznetsov), aluna@inaoep.mx (A.L. Castellanos), danielslfce@yahoo.com.mx (D.S. Lucero).
[1]Tel.: +7 812 552 6314.

0030-4026/$ - see front matter © 2009 Elsevier GmbH. All rights reserved.
doi:10.1016/j.ijleo.2009.02.015

effects, such as soliton and parametric phenomena, all-optical multi-stability, etc. [1,2]. In this paper, the practical potentials related to exploiting the nonlinear process of wave heterodyning in a medium with dispersive losses are considered. In the case of wave heterodyning, beneficial analogue information incorporated into the spectrum of a signal gets converted from a high-frequency signal wave to a difference-frequency wave, so that just spectral components peculiar to the resulting difference-frequency wave are exploited during subsequent optical data processing. Usually, the precision of both spectral and frequency measurements for signals is determined by the uncertainty in the energy or momentum inherent in a photon localized in the interaction area [3]. Due to the dispersion of losses, heterodyning leads to increase in the characteristic length and/or time of propagation for the converted signal in that medium and to significant improvement in the accuracy of the optical data processing, because both spectral and frequency resolutions are in inverse proportion to the length or time of acousto-optical interaction. Here, we are reporting our investigations of the co-directional collinear longitudinal acoustic wave heterodyning through acousto-optic technique and its possible application to a real-time acousto-optical analysis of the frequency spectrum belonging to ultra-high-frequency (UHF) radio-wave analogue signals. The character of our studies is directly connected with actual absence of sufficiently effective acousto-optical materials suitable for processing ultra-high-frequency radio-wave analogue signals. Exploiting the introduced approximation, the theory of wave heterodyning in a medium with the dispersive losses has been progressed. Then, the developed theory was applied to our experiments directed to increase the accuracy of acousto-optical spectrum analyzers working in the UHF range. In fact, optical data processing with essentially improved frequency resolution has been experimentally observed within exploiting the created new acousto-optical cell based on exploiting rather effective lead molybdate crystal with resonant frequencies lying in a frequency range where conventional cell made of this material is not profitable. The obtained results confirm principally the advantages of our approach.

2. Formulating the problem: frequency performances and resolution of the Bragg acousto-optical deflector operating in a one-phonon Bragg normal light-scattering regime

Let us start from preliminary estimations of the frequency bandwidth Δf, the frequency resolution δf, and the number N of resolvable spots inherent in the Bragg acousto-optical deflector operating in a one-phonon normal light-scattering regime. A one-phonon non-collinear light scattering in isotropic medium, see Fig. 1a, is associated with the Bragg condition [4,5]

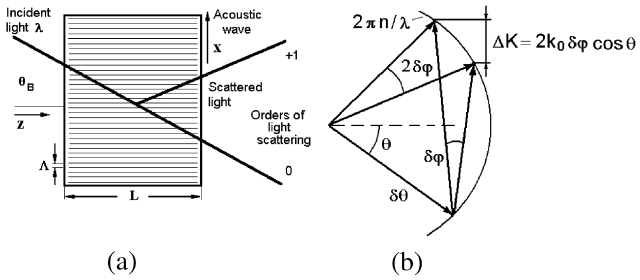

Fig. 1. A one-phonon normal light-scattering regime: principal schematic arrangement for the Bragg light scattering (a) and the corresponding vector diagram determining the frequency bandwidth (b).

$$\sin\theta = -\frac{K}{(2k_0)} = -\lambda\frac{f}{(2nV)} \tag{1}$$

for normal process without changing the state of light polarization. Here, θ is the Bragg angle of light scattering, k_0 and λ are the wave number and the wavelength of light, respectively, n is the corresponding refractive index, K, f, and V are the wave number, carrier frequency, and phase velocity of the acoustic wave, respectively. The corresponding wave vector diagram is depicted in Fig. 1b. The frequency bandwidth of acousto-optical interaction Δf can be estimated through differentiating this Bragg condition in Eq. (1) as $\Delta f = \Delta\theta(2nV/\lambda)\cos\theta$, where $\Delta\theta$ is the variation of the angle of light incidence associated with the variation of the acoustic frequency Δf needed to provide the Bragg condition. In the case of light modulation, we have usually the geometry of interaction with rather wide optical beam, whose angle of spreading $\delta\theta$ is small, and rather narrow aperture of the acoustic beam, whose angle of spreading is $\delta\varphi \approx (V/fL) \gg \delta\theta$, where L is the length of acousto-optical interaction, see Fig. 1a. Assuming that $\delta\varphi \approx \Delta\theta$ and $\cos\theta \approx 1$, we yield the following approximation

$$\Delta f \approx \frac{2nV^2}{\lambda L f} \tag{2}$$

for the bandwidth of a normal Bragg acousto-optical interaction in isotropic medium. This approximate equality follows geometrically from the plot in Fig. 1b, because $\Delta K = 2\pi(\Delta f)/V$ and $2k_0\delta\varphi\cos\theta \approx 4\pi nV/(\lambda L f)$.

Generally, the momentum p of a photon is connected with the wave number k as $p = hk/(2\pi)$, where h is the Planck constant, so an uncertainty $\delta p = h(\delta k)/(2\pi)$ in the momentum is related to the uncertainty in the wave number δk of a photon. The same view is true, if one will consider the phonons. Namely, the momentum P of a phonon is connected with the wave number K as

$P = hK/(2\pi)$ and an uncertainty $\delta P = h(\delta K)/(2\pi)$ in the momentum related to the uncertainty in the wave number δK of a phonon. Then, because the phonon wave number is $K = 2\pi f/V$, one can note that an uncertainty of the phonon wave number, in its turn, can be explained in terms of an uncertainty in the phonon frequency δf as $\delta K = 2\pi(\delta f)/V$. The limiting case of just Bragg light scattering in acousto-optics is determined by the well-known [4–6] dimensionless inequality for the Klein–Cook parameter

$$Q = \frac{\lambda f^2 L}{V^2} \gg 1. \tag{3}$$

In this limit an uncertainty in the momentum of the issuing photon is characterized by the relation $\delta p \approx \delta p$, and, consequently, $\delta k \approx \delta K$, because they both are localized inside the same spatial area determined by the aperture D. Together with this, the value of δk is significantly smaller than the photon wave number variation connected with scattering from the order j to the order $j+1$, i.e. $|\vec{k}_{j+1} - \vec{k}_j| \approx K \gg \delta K \approx \delta k$. By this is meant that the wave numbers of both the photons and the phonons are well determined in the Bragg limit of acousto-optical interaction. Due to the Heisenberg uncertainty principle [3] proclaims that $\delta p \delta x \sim h$ with $\delta x \approx D$, one can found that

$$\delta f \approx \frac{V}{D} = T^{-1}, \tag{4}$$

where T is the time of passing the acoustic wave through the aperture D. Just this value determines the frequency resolution of acousto-optical modulator operating in a one-phonon Bragg normal light-scattering regime. The number N of resolvable spots in the regime under consideration is given by the ratio

$$N = \frac{\Delta f}{\delta f} = T\Delta f. \tag{5}$$

In high-frequency devices, the value of N is restricted by both the geometrical factors and the acoustic attenuation in a medium. The first geometric factor is the maximal aperture D of a deflector. In connection with this, one can estimate the maximal bandwidth as $\Delta f \approx f_0/2$, where f_0 is the central carrier frequency of the acoustic wave, and obtain the first limitation

$$N_1 \leqslant \frac{Df_0}{2V}. \tag{6}$$

The second factor is determined by the acoustic beam spreading. One can assume that the aperture D of that deflector belongs to the near zone of radiation from the piezo-electic transducer, whose size can be taken to be equal to L, so that $D \approx L^2 f_0/(2V)$. This relation leads to $L = nV^2 Q/(2\pi\lambda f_0^2)$ and to the second limitation

$$N_2 \leqslant \left(\frac{nVQ}{4\pi\lambda f_0}\right)^2. \tag{7}$$

The third principal limitation is conditioned by acoustic attenuation. It can be also represented as a function of f_0. Let us use the factor Γ_0 of acoustic attenuation expressed in [dB/(cm GHz^2)], so that χ-dB level of attenuation will require the aperture $D \leqslant \chi\Gamma_0^{-1} f_0^{-2}$. Substituting this formula into Eq. (6), one can find

$$N_3 \leqslant \frac{\chi}{2\Gamma_0 V f_0}. \tag{8}$$

Thus, the number of resolvable spots is restricted by a triplet of the above-mentioned independent limitations. To make illustrating numerical estimations one can take, for example, an acousto-optical deflector made of such widely exploited crystalline material as lead molybdate ($PbMoO_4$). In this particular case of a one-phonon Bragg normal light scattering, one can take the following values inherent in this crystal: $V = 3.63 \times 10^5$ cm/s, $\lambda = 633$ nm, $n = 2.26$, and $\Gamma_0 = 15$ dB/(cm GHz^2) [4,7]. The numerical estimations have been realized for apertures $D = 1{-}4$ cm; attenuation factors along the total aperture $\chi = 4$ and 6 (dB/aperture), and the Klein–Cook parameter $Q = 2\pi$, 3π, and 4π, providing just the Bragg regime of light scattering, see Fig. 2. It is seen that a lead molybdate deflector with $D \approx 2$ cm, $Q = 2\pi$, and $\chi < 4$ (dB/aperture) is capable to provide $N \approx 700$ resolvable spots with a potential frequency resolution δf of approximately 180 kHz in the frequency bandwidth close to 120 MHz at a central frequency f_0 of about 250 MHz. Together with this, using Fig. 2 one can conclude that conventional lead molybdate deflector even with an aperture of 1 cm is not operable at the carrier frequencies exceeding 600 MHz. Thus, now one can formulate the problem facing this article. Taking alone a given lead molybdate optical deflector with the given aperture $D = 2$ cm, is it possible to keep the same number of resolvable spots with the same potential

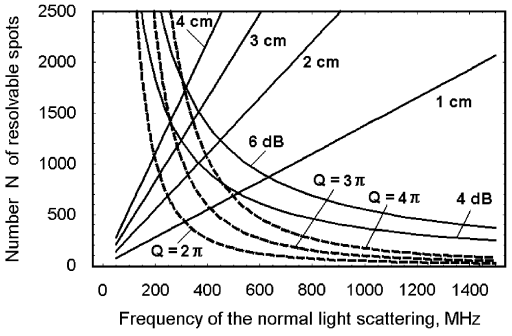

Fig. 2. The combined diagram illustrating effect of a triplet of the restricting factors. The solid straight lines are related to N_1, the chosen apertures D are equal to 1, 2, 3, and 4 cm. The dashed lines regards to N_2 in the particular cases of $Q = 2\pi$, 3π, and 4π. The solid hyperbolic-like falling curves illustrate N_3 and reflect contributions of the acoustic attenuation with total losses of 4 and 6 dB along the optical aperture.

frequency resolution in the same frequency bandwidth at a significantly increased central carrier frequency f_0 exceeding the above-mentioned 600 MHz? The main goal of our considerations is to give definitely positive answer to this question under condition of exploiting the collinear acoustic wave heterodyning in the taken optical deflector.

3. Co-directional collinear propagation and interaction of the longitudinal acoustic waves of finite amplitudes

It is well known that co-directional collinear propagation of longitudinal acoustic waves of finite amplitudes in isotropic media and along the acoustic axes in crystalline materials, which do not have the group-velocity dispersion, but have the dispersive losses, is governed by the Burgers equation for the normalized distortion $\xi = D_a/D_0$ [8]

$$\frac{\partial \xi}{\partial y} = B\xi\frac{\partial \xi}{\partial \theta} + \frac{\partial^2 \xi}{\partial \theta^2}. \tag{9}$$

Here, D_a is the amplitude of distortion, D_0 is the amplitude of acoustic pump distortion, $\theta = \omega(t - x/V)$, $y = \alpha_p x$, $\omega = 2\pi f$, V, and α_p are the cyclic frequency, velocity, and logarithmic attenuation of the pump acoustic wave. Then, the parameter $B = -\omega\Gamma D_0/(2\alpha_P V)$ describes a ratio of the acoustic nonlinearity to the acoustic dissipation; Γ is the nonlinearity constant. Fig. 3 illustrates arranging the interacting beams of the acoustic waves in a cell.

Broadly speaking, Eq. (9) can be analytically solved in its general form with arbitrary boundary conditions due to well-known Hopf–Cole substitution converting the nonlinear Burgers equation into linear heat conduction equation [8]. However, very cumbersome form of such a solution does not give a chance to perform the subsequent harmonic analysis. The spectral approach, when the project of solution has a given form, does not lead to a success as well, because in this case one has to solve an infinite set of the combined nonlinear equations. That is why the most worthwhile way is connected with finding an approximate solution by the method of successive approximations. The needed approximate solutions can be obtain rather fast when the parameter B is not too large. In so doing, let us take the boundary condition to Eq. (9) in the form of a superposition of two longitudinal waves. One of them with unit amplitude and the cyclic frequency $\omega_P = 2\pi f_P$ can be considered as a pump, while the other wave represents a signal with an amplitude of δ and a cyclic frequency of $\omega_S = 2\pi f_S$, so that

$$\xi(y = 0, \theta) = \sin(\theta + \psi) + \delta\sin(\gamma\theta), \tag{10}$$

where $\gamma = \omega_S/\omega_P$, ψ is the phase shift between the signal and pump, $\delta = \sqrt{P_S/P_P}$, P_P and P_S are the acoustic power densities for the pump and signal, respectively. Here, we restrict ourselves by the regime of non-degenerate acoustic interaction. Substituting Eq. (10) into Eq. (9), one can find the zero approximation solution describing the propagation of two attenuating non-interacting waves as $\xi^{(0)} = \exp(-y)\sin(\theta + \psi) + \delta\exp(-\gamma^2 y)\sin(\gamma\theta)$. Now, using $\xi^{(0)}$ in the nonlinear term of Eq. (9), one can estimate the first approximation solution as

$$\begin{aligned}\xi^{(1)} = \xi^{(0)} &= a^{(1)}_{P+P}\sin[2(\theta + \psi)] + a^{(1)}_{S+S}\sin(2\gamma\theta) \\ &+ a^{(1)}_{S+P}\sin[(\gamma + 1)\theta + \psi] + a^{(1)}_{S-P}\sin[(\gamma - 1)\theta + \psi].\end{aligned} \tag{11}$$

Here, $a^{(1)}_{P+P} = -(B/4)[\exp(-2y) - \exp(-4y)]$ is the second harmonic amplitude of an acoustic pump wave, $a^{(1)}_{S+S} = -(B\delta^2/4\gamma)[\exp(-2\gamma^2 y) - \exp(-4\gamma^2 y)]$ is the amplitude of the second harmonic of an acoustic signal wave. Then, a pair of the following expressions: $a^{(1)}_{S+P} = -(B\delta(\gamma + 1)/4\gamma)[\exp(2\gamma y) - 1]\exp[-y(1 + \gamma)^2]$ and $a^{(1)}_{S-P} = (B\delta(\gamma - 1)/4\gamma)[1 - \exp(-2\gamma y)]\exp[-y(1 - \gamma)^2]$ give the amplitudes of acoustic waves with the combined and difference frequencies. Exploiting quite similar technique and neglecting the terms of the order of δ^3, one can calculate approximate solutions of the second order. In the particular case of the second approximation for acoustic wave amplitude with the difference frequency, one can write

$$\begin{aligned}a^{(2)}_{S-P} = &\frac{B\delta(\gamma - 1)}{4\gamma}\exp[-y(\gamma - 1)^2] \\ &\times\left\{[1 - \exp(-2\gamma y)] + \frac{B^2(\gamma + 1)}{16}\left[\frac{1 - \exp[-2y(\gamma + 1)]}{\gamma + 1}\right.\right. \\ &+ \frac{1 - \exp[-4y(\gamma + 1)]}{2(\gamma + 1)} - \frac{1 - \exp[-2y(\gamma + 2)]}{\gamma + 2} \\ &\left.\left. - \frac{1 - \exp[-2y(2\gamma + 1)]}{2\gamma + 1}\right]\right\}.\end{aligned} \tag{12}$$

In the case, when the nonlinearity does not exceed the dissipation, i.e. if $B^2 \leqslant 1$ and $\delta^3 \ll 1$, an additional acoustic wave with the difference frequency can be

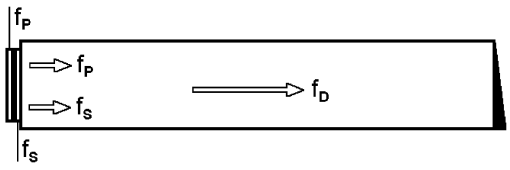

Fig. 3. Arranging the interacting acoustic beams consisting of the longitudinal acoustic waves of finite amplitudes in a cell.

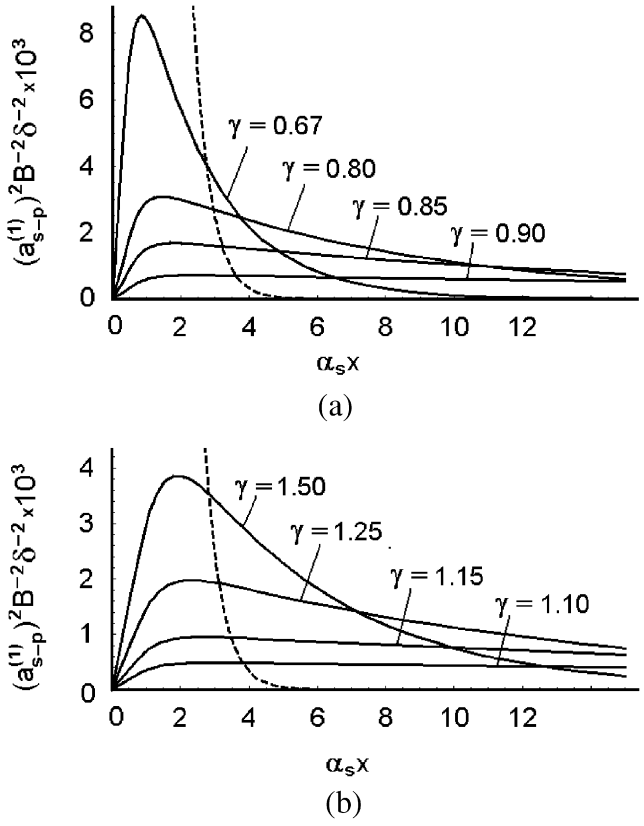

Fig. 4. The spatial normalized plots of an additional acoustic wave power with the different frequencies in the case of $B \leqslant 1$ and $\delta^3 \ll 1$ for various values of the parameter γ: (a) $\gamma < 1$; (b) $\gamma > 1$.

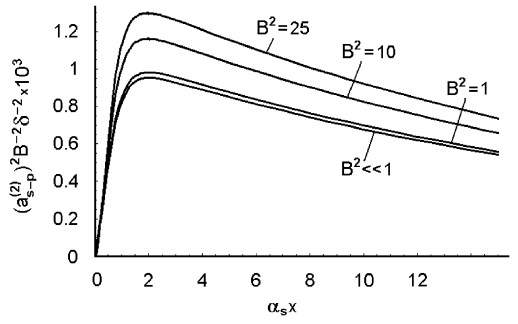

Fig. 5. The spatial normalized plots of an additional acoustic wave power with the different frequencies in the case of $\gamma = 1.15$ and $\delta^3 \ll 1$ for various values of the parameter B.

characterized by the first-order solution as well. After squaring and normalizing, one obtains

$$\left(a_{S-P}^{(1)}\right)^2 B^{-2}\delta^{-2} = \left[\frac{1}{4\gamma}(\gamma-1)\right]^2 E_i^2(\gamma, \alpha_S x), \tag{13}$$

$$E_i(\gamma, \alpha_S x) = \left[1 - \exp\left(-\frac{2\alpha_S x}{\gamma}\right)\right]\exp\left[-\alpha_S x\left(\frac{\gamma-1}{\gamma}\right)^2\right]. \tag{14}$$

Here, the relations $y = \alpha_P\, x = \alpha_S \gamma^{-2} x$ were used; α_S is logarithmic decrement characterizing acoustic attenuation the signal acoustic wave. The spatial dependences reflecting Eq. (14) are presented in Fig. 4. For comparison, these plots include the exponential dependence $\exp(-2\alpha_S x)$, which describes decrease in the acoustic signal power in zero approximation with $B = 1$. One can see that the distributions of acoustic power on these plots are as more uniform as values of the parameter γ are closer to unity. However, therewith the intensity of an additional acoustic wave decreases directly proportional to $(\gamma-1)^2$.

It follows from Eq. (12) that the correction to the first-order solution $a_{S-P}^{(1)}$ increases the amplitude of additional acoustic wave. By this it mean that when B^2, which is directly proportional to the inputting power of acoustic pump, grows by ten times, the acoustic power of an additional wave increases by more then ten times, see Fig. 5. Nevertheless, including the obtained corrections of the second order in the solution of the first order changes nothing in the character of these dependences.

The power density P_i inherent in an additional acoustic wave of the difference frequency in the first approximation can be explained in dimensional values as

$$P_i(\gamma, \alpha_S x) = P_P P_S \left(\frac{f_i}{f_P f_S}\right)^2 m E_i^2(\gamma, \alpha_S x), \tag{15}$$

where $f_i = |f_P - f_S|$. Then, the value

$$m = \frac{1}{8\rho V}\left(\frac{\pi\Gamma}{V^2\Gamma_0}\right)^2 \tag{16}$$

Table 1. Physical properties of some materials appropriate for the acousto-optic cell, see [4,7].

Material	H_2O	C_2H_5OH	$PbMoO_4$	As_2S_3
Material density ρ (g/cm^3)	1.00	0.787	6.95	3.20
Direction of propagation for the longitudinal acoustic waves	Arbitrary	Arbitrary	[0 0 1]	Arbitrary
Velocity of propagation $V \times 10^{-5}$ (cm/s)	1.49	1.15	3.62	2.60
Modulus of the nonlinear parameter $\lvert\Gamma\rvert$	8.0	12.3	17.5	21.5
Factor of the acoustic attenuation $\Gamma_0 \times 10^{18}$ (s^2/cm)	552	1247	3.45	39.1
Acoustic quality factor $m \times 10^{-6}$ (s/g)	3.53	7.545	725	98.1
Acousto-optic figure of merit $M_2 \times 10^{18}$ (s^3/g)	126	543	36.3	429

determines the efficiency of generating an additional difference-frequency acoustic wave in a medium and takes into account the factor Γ_0 characterizing the attenuation of acoustic waves. Usually, the acoustic attenuation is mentioned in bibliography in units of [dB/(cm GHz^2)], but Eq. (16) needs it in the form

$$\Gamma_0(s^2/\mathrm{cm}) = 0.23\,\Gamma_0[\mathrm{dB}/(\mathrm{cm\,GHz}^2)]10^{-18}. \tag{17}$$

Physical parameters for a few materials available for acoustic wave heterodyning are presented in Table 1.

Acousto-optical technique is one of the most sensitive methods to detect various acoustic signals. In connection with this, it would be worthwhile to discuss the efficiency I of light scattering by an additional acoustic wave in the linear regime of rather weak acoustic signals. In this particular case [4,5],

$$I = \frac{\pi^2 M_2 P_i L^2}{2\lambda^2}, \tag{18}$$

where λ is the optical wavelength. Now, we can exploit Eq. (14) and (15) to rewrite Eq. (17) as

$$I = \frac{\pi^2 M_2 L^2}{2\lambda^2} P_P P_S \left(\frac{f_i}{f_P f_S}\right)^2 m E_i^2(\gamma, \alpha_S x), \tag{19}$$

which determines the combined efficiency of the acousto-optical cell in terms of light scattering.

4. Experimental verifications and modeling

The obtained theoretical results related to collinear interaction of longitudinal acoustic waves were examined experimentally via exploitation of the acousto-optic technique. The main attention was paid to the process of generating an additional acoustic wave with the difference frequency. In so doing, the experimental set-up, whose optical part is presented in Fig. 6, was used. The collimated laser light beam with a wavelength of 633 nm was directed at the rotating mirror placed at the focus of the cylindrical lens 2. Rotation of this mirror provided the incidence of light beam at an arbitrary point of the acoustic duct. Light, scattered by an additional acoustic wave, was redirected to photo-detector placed at the focal plane of the cylindrical lens 1. At this step, one has to say that the analytical

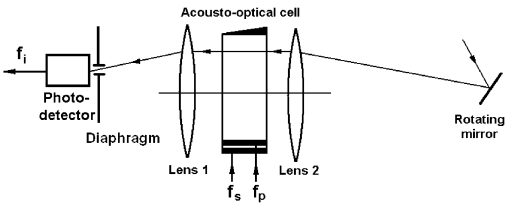

Fig. 6. Optical scheme of the experimental set-up.

Fig. 7. Acousto-optical cell with two piezo-electric transducers and with liquid medium represented by ethanol.

calculations allow the principal opportunity for experimental simulation of the desirable collinear interaction between high-frequency acoustic waves passing along the wave axes in anisotropic solid states through studying similar processes at low frequencies in isotropic media with acceptable characteristics, namely parameters of acoustic nonlinearity, acoustic attenuation, acoustic and acousto-optical figures of merit. In particular, the performed investigations were oriented on experimental simulation of co-directional collinear interaction for acoustic waves of about 1 GHz, for example, in lead molybdate crystal ($PbMoO_4$) through studying similar process in the acousto-optical cell exploiting ethanol (C_2H_5OH) at the frequencies of about 30–80 MHz, see Fig. 7.

In fact, the experiments were carried out at the following pairs of the modeling frequencies in ethanol:

$$\begin{aligned}
&f_S = 30\,\mathrm{MHz}, \quad f_p = 47.2\,\mathrm{MHz}, \quad f_i = 17.2\,\mathrm{MHz}, \quad \gamma = 0.64;\\
&f_S = 57.3\,\mathrm{MHz}, \quad f_p = 82\,\mathrm{MHz}, \quad f_i = 24.7\,\mathrm{MHz}, \quad \gamma = 0.70;\\
&f_S = 47\,\mathrm{MHz}, \quad f_p = 57\,\mathrm{MHz}, \quad f_i = 10\,\mathrm{MHz}, \quad \gamma = 0.82;\\
&f_S = 28\,\mathrm{MHz}, \quad f_p = 31\,\mathrm{MHz}, \quad f_i = 3\,\mathrm{MHz}, \quad \gamma = 0.91.
\end{aligned} \tag{20}$$

Using Eq. (17), one can find that the experimental parameters of the modeling and real media are connected with each other as

$$\begin{aligned}
&(a)\quad f_S^2 = \frac{\Gamma_{0,M}}{\Gamma_0} f_{S,M}^2, \quad (b)\quad \gamma = \gamma_M,\\
&(c)\quad \frac{P_P P_S}{\lambda^2 H^2} = \frac{\mu_M \Gamma_{0,M}}{\mu \Gamma_0}\left(\frac{P_P P_S}{\lambda^2 H^2}\right)_M,
\end{aligned} \tag{21}$$

where the index "M" is related to parameters of the modeling process. In the case of, for example, a lead

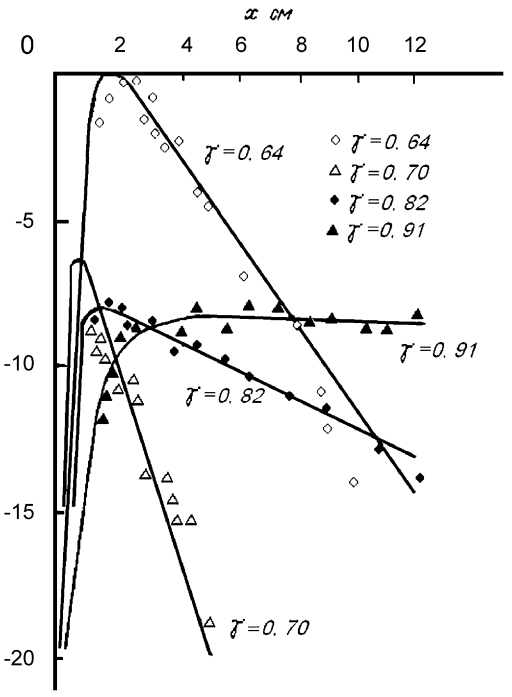

Fig. 8. Normalized spatial dependences for the efficiency I of light scattering by the difference-frequency acoustic wave.

molybdate crystal, these data are represented by

$$\begin{aligned} &f_S = 0.53\,\text{GHz}, \quad f_p = 0.84\,\text{GHz}, \quad f_i = 0.31\,\text{GHz}, \quad \gamma = 0.64;\\ &f_S = 1.02\,\text{GHz}, \quad f_p = 1.46\,\text{GHz}, \quad f_i = 0.44\,\text{GHz}, \quad \gamma = 0.70;\\ &f_S = 0.83\,\text{GHz}, \quad f_p = 1.01\,\text{GHz}, \quad f_i = 0.18\,\text{GHz}, \quad \gamma = 0.82;\\ &f_S = 0.49\,\text{GHz}, \quad f_p = 0.54\,\text{GHz}, \quad f_i = 0.05\,\text{GHz}, \quad \gamma = 0.91. \end{aligned} \tag{22}$$

The normalized data reflecting the coordinate dependences of light-scattering efficiency by an additional acoustic wave are presented in Fig. 8. The points are experimental data, while the solid lines explain the corresponding calculations. The comparison of these data illustrates the possibility of applying the elaborated analytical method to describe co-directional collinear interaction of the longitudinal high-frequency acoustic waves, in particular, to the process of exiting an additional acoustic wave with the difference frequency and its visualizing via acousto-optic technique.

5. Practical estimations and proof-of-principle experimental studies of the potentials peculiar to optical spectrum analysis with a novel lead molybdate crystalline acousto-optical cell

In the first approximation, the normalized amplitude of the difference-frequency carrier acoustic wave passing along the optical aperture of a cell is given by Eq. (13),

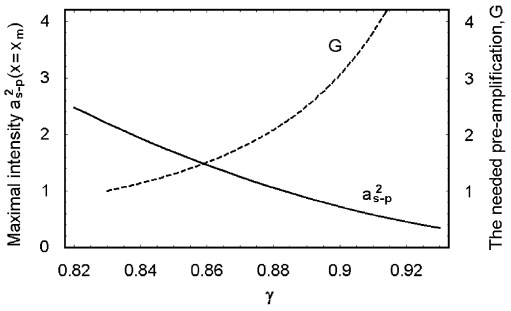

Fig. 9. The plots of $a^2_{s-p}(x = x_m)$ — solid line, and $G(\gamma)$ ---- dashed line, for magnitudes of γ practically usable in the wave heterodyning.

which can be rewritten as

$$a_{S-P}(x) = \left(\frac{\gamma-1}{4\gamma}\right)[1-\exp(-2\gamma\alpha_P x)]\exp[\alpha_P x(1-\gamma)^2]. \tag{23}$$

Using Eq. (23), one can determine the point x_m associated with a maximum of the normalized amplitude distribution along the cell as

$$x_m = \left(\frac{-1}{2\alpha_P\gamma}\right)\ln\left[\frac{(1-\gamma)^2}{1+\gamma^2}\right]. \tag{24}$$

The magnitude of this maximum can be estimated as

$$a_{S-P}(x = x_m) = \frac{\gamma-1}{2(1+\gamma^2)}\exp\left\{\frac{(1-\gamma)^2}{2\gamma}\ln\left[\frac{(1-\gamma)^2}{1+\gamma^2}\right]\right\}. \tag{25}$$

It is seen from Eq. (25) and Fig. 4 that $a^2_{S-P}(x = x_m)$ is the decreasing function of γ, see the solid line in Fig. 9. However, such a dependence on γ leads to a non-uniformity of distributing signals associated with various difference-frequency components in a cell. To compensate this non-uniformity one can suggest to exploit the additionally needed pre-amplification $G(\gamma)$, which is shown by dashed line in Fig. 9 and can be calculated as

$$G(\gamma) = \frac{a^2_{S-P}(x = x_m, \gamma = \gamma_0)}{a^2_{S-P}(x = x_m, \gamma)}, \tag{26}$$

where γ_0 is an initially selected, minimal, and fixed value of the ratio γ.

Decreasing the normalized intensity $a^2_{S-P}(x)$ of the difference-frequency acoustic wave down to a level of -3 dB along the cell's optical aperture at a point x_D gives the equality $a_{S-P}(x = x_D) = (1/\sqrt{2})a_{S-P}(x = x_m)$ in terms of the amplitudes, so that

$$x_D = \frac{-1}{2\alpha_P(1-\gamma)^2}\left(\ln\left(\frac{\gamma\sqrt{2}}{1+\gamma^2}\right) + \left\{\frac{(1-\gamma)^2}{2\gamma}\ln\left[\frac{(1-\gamma)^2}{1+\gamma^2}\right]\right\}\right). \tag{27}$$

In fact, the value of x_D determines the total length of acousto-optical cell with the collinear wave heterodyning.

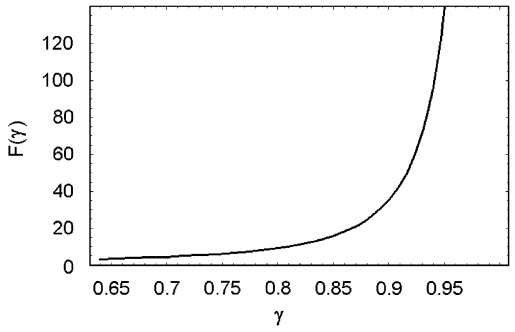

Fig. 10. The plot of $F(\gamma)$ for magnitudes of γ practically usable in the wave heterodyning.

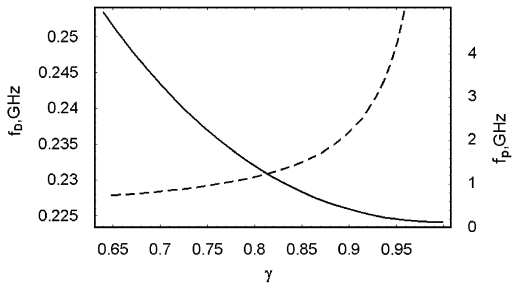

Fig. 11. Plots for the pump frequency f_p (dashed line) and the difference frequency f_D (solid line) related to Eqs. (29) versus γ for magnitudes of γ practically usable in the wave heterodyning.

Now, an active part D of the cell's optical aperture available for optical processing can be found as

$$\text{(a)}\quad D = x_D - x_m = \frac{F(\gamma)}{\alpha_P},$$

$$\text{(b)}\quad F(\gamma) = \frac{1}{(1-\gamma)^2}\ln\left(\frac{1+\gamma^2}{\gamma\sqrt{2}}\right). \tag{28}$$

The plot of $F(\gamma)$ for values of γ neighboring unity and capable to be practically usable in the wave heterodyning is presented in Fig. 10.

Because $\alpha_P = 0.23\Gamma_0 f_P^2$ (cm^{-1}), see Eq. (17), the following expression for the pump frequency f_p and for the difference frequency $f_D = f_P - f_S = f_P(1-\gamma)$ appear

$$\text{(a)}\quad f_P = \sqrt{\frac{F(\gamma)}{0.23\Gamma_0 D}},\quad \text{(b)}\quad f_D = (1-\gamma)\sqrt{\frac{F(\gamma)}{0.23\Gamma_0 D}}. \tag{29}$$

In the particular case of a lead molybdate ($PbMoO_4$) crystal ($\Gamma_0 = 15\,\mathrm{dB/cm\,GHz^2}$) with the active optical aperture $D = 2\,\mathrm{cm}$, one can obtain from Eqs. (29) the following diagrams, see Fig. 11.

These dependencies allow the following estimation for practical realization. Let us take the upper difference-frequency as $f_{UD} = 230\,\mathrm{MHz}$ and the lower magnitude of γ as $\gamma_L = 0.83$, so that the pump frequency will be $f_p = 1350\,\mathrm{MHz}$ and the lower signal frequency will be

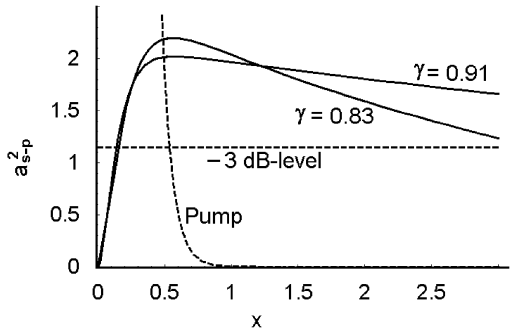

Fig. 12. A non-uniformity in the distributions of signals associated with various difference-frequency components in the lead molybdate cell.

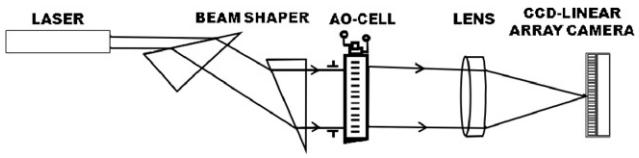

Fig. 13. Schematic arrangement of a prototype for the acousto-optical spectrum analyzer.

$f_{LS} = 1120\,\mathrm{MHz}$. Then, one can choose the bandwidth Δf of analysis, for example, in the range of 110 MHz, which leads to the lower difference-frequency $f_{LD} = 120$ MHz, the upper signal frequency $f_{US} = 1230\,\mathrm{MHz}$, and the upper magnitude $\gamma_U = 0.91$. These estimations are conditioned by the relations

$$\text{(a)}\quad f_{UD} = f_P - f_{LS} = f_P(1-\gamma_L),$$
$$\text{(b)}\quad f_{LD} = f_P - f_{US} = f_P(1-\gamma_U). \tag{30}$$

It is seen from Fig. 2 that direct exploitation of similar lead molybdate cell with the active optical aperture $D = 2\,\mathrm{cm}$ at the signal frequencies of about 1100–1200 MHz is definitely impossible. Nevertheless, applying the collinear acoustic wave heterodyning allows to operate on these ultra-high carrier frequencies and to obtain the number of resolvable spots of about $N = \Delta f/\delta f \approx 610$. The above-mentioned non-uniformity in the distributions of signals associated with various difference-frequency components in the lead molybdate cell under consideration are illustrated in Fig. 12.

Exploiting the modeling procedure discussed in Section 4 and the above-listed estimations, a novel solid-state acousto-optical cell had been designed and used in the standard scheme of a prototype for the acousto-optical spectrum analyzer of ultra-high-frequency radio-signals, see Fig. 13. This scheme includes a rather powerful laser ($\lambda = 440\,\mathrm{nm}$, the issuing optical power exceeds 100 m W), a two-prism beam shaper, large-aperture achromatic doublet lens, and a 3000-pixel CCD linear array photo-camera. A lead molybdate

($PbMoO_4$) single crystal of 25 mm in length, oriented along the [0 0 1]-axis for an acoustic beam along [1 0 0]-axis for an optical beam [4,5,7], was used in that cell. The cell completed with a pair of electronic input ports for the pump and signal on one of its facets as well as with acoustic absorber on the opposite facet.

This crystalline material was chosen because of its high value of the relative acousto-optic figure of merit that can be characterized by a value of $M_2 \approx 36.3 \times 10^{-18}\,s^3/g$ for both possible eigen-states of light polarization in this tetragonal crystal and its rather high acoustic interaction efficiency for collinear longitudinal waves in the [0 0 1]-direction described by $|\Gamma| = 17.5$ [7]. As it was noted in Section 1, the range of applicability for similar lead molybdate cell in conventional design is practically limited by frequencies of the order of 300–400 MHz. The piezo-electric transducer with an interaction length of 10 mm, generating the signal wave with power density of about 100 mW/mm^2, was made of a thin ($Y+36^\circ$)-cut lithium niobate, so that it excited purely longitudinal acoustic wave, with conversion losses of about 2 dB at its resonant frequency close to 1160 MHz. The single-frequency pumping longitudinal acoustic wave with the power density of up to 600 mW/mm^2 was generated at a carrier frequency of approximately 1350 MHz, so that the case of $\gamma \in [0.80, 0.93]$ had been experimentally realized. During the experiments, we placed a diaphragm in a few millimeter vicinity of the piezo-electric transducers area (about 15% of the total aperture) to minimize the effect of this area, where an increase in the power of difference frequency waves takes place. Consequently, the working optical aperture of a cell slightly exceeds 2 cm. The bandwidth of that prototype was about 120 MHz. The efficiency of light scattering by an additional acoustic wave at the difference-frequency was slightly exceeding 1%. Fig. 14 shows the digitized oscilloscope traces of amplitude–frequency distribution peculiar to that prototype with the acousto-optical cell based on the collinear wave heterodyning. The digitized trace of this distribution had been recorded by a multi-pixel CCD linear array photo-camera through connecting the input signal port of a cell at an ultra-high-frequency radio-wave sweep-generator and fulfilling the acoustic wave heterodyning in a lead molybdate crystal. For a signal at the resulting currier difference-frequency of about 230 MHz, the attenuation is close to 3 dB over the total cell aperture, while for a signal acoustic wave at the original frequency 1120 MHz the attenuation exceeds 36 dB along that aperture, which is perfectly unacceptable in practice. Within the second set of experimental tests, we examined the resolution of spectrum analyzer with the cell exploiting the acoustic wave heterodyning. The obtained data corresponds to a frequency resolution of about $\delta f \approx 200$ kHz and $N \approx 600$, see Fig. 15. This digitized trace had been recorded in the focal plane of lens, see Fig. 13, via applying just a single-frequency excitation at the input signal port of a novel cell under consideration.

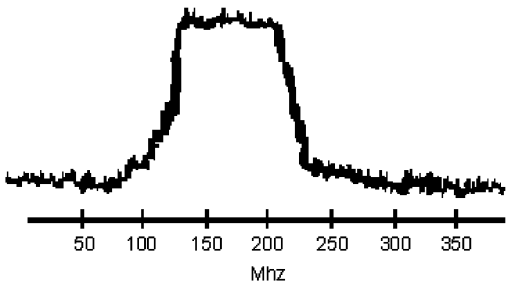

Fig. 14. The digitized oscilloscope trace of the amplitude–-frequency distribution inherent in acousto-optical cell based on the longitudinal acoustic wave heterodyning in a lead molybdate crystal.

Fig. 15. The digitized profile of individual resolvable spot inherent in that crystalline cell with the most non-uniform ($\gamma_L = 0.83$) distribution of the difference-frequency acoustic waves along the cell's aperture; horizontal lines are spaced here by an interval of 2.5 dB.

6. Conclusion

We have investigated both theoretically and experimentally the phenomenon of a co-directional collinear wave heterodyning, considering the particular case of interaction of the longitudinal acoustic waves of finite amplitudes. In so doing, the acousto-optical technique has been exploited. Possible applications of this phenomenon to the acousto-optical spectrum analysis of the UHF radio-wave signals have been tested as well. At the beginning, the experimental modeling of the acoustics wave mixing process in solids via application of acousto-optical cell based on liquid material, namely liquid ethanol, which makes possible the simplest option for realizing the corresponding cells with the needed parameters, has been examined.

Then, the obtained results of analysis and modeling have been used in our experiments directed to increase the performance data of acousto-optical devices. In particular, an opportunity to implement the acousto-optical data processing with the acoustic wave heterodyning has been experimentally demonstrated utilizing the acousto-optical cell made of a lead molybdate crystal.

The presented results demonstrate the possibility of applying co-directional collinear interaction of the longitudinal acoustic waves to resolve one of the problems related to acousto-optical spectrum analysis of just the UHF radio-wave signals. Devices of this sort provide an improved frequency resolution in that bandwidth of the working frequencies, where conventional acousto-optical cells made of given materials cannot operate. The functional scheme of the devices under proposal differs from the scheme for spectrum analysis with the electrical heterodyning that it does not require a mixer for microwave signals or a powerful intermediate-frequency amplifier. Both the acoustic wave heterodyning and the amplification of signal waves at the difference frequencies occur in a single solid-state circuit using the energy from the acoustic pump. Furthermore, the required relative frequency bandwidths of both the piezo-electric transducers on a facet of a cell are considerably small, so that the fabrication of these transducers could be simplified. The proposed scheme of acousto-optic spectrum analyzer may prove to be the most effective at frequencies above 1 GHz or more. Consequently, the results of these studies should also be thought of as an experimental modeling for gigahertz-range devices, where the choice of materials for effective acousto-optic cells is rather limited because of the increased (in fact, directly proportional to the currier acoustic frequency squared) attenuation for acoustic waves.

Acknowledgments

The work was financially supported by the CONACyT, Mexico (Project no. 61237-F). Also, the authors thank Dr. Luis Carrasco (INAOE, Mexico) for his stimulating discussions related to developing and implementing the specialized acousto-optical equipment providing a high-resolution spectrum analysis of radio-wave signals from the Mexican Large Millimeter Telescope.

References

[1] Yu.S. Kivshar, G.P. Agrawal, Optical Solitons: from Fibers to Photonic Crystals, Academic Press, New York, 2003.
[2] N.N. Akhmediev, A. Ankiewich, Solitons: Nonlinear Pulses and Beams, Chapman & Hall, London, 1997.
[3] P.A.M. Dirac, The Principles of Quantum Mechanics, forth ed., Oxford University Press, Oxford, 1999.
[4] V.I. Balakshy, V.N. Parygin, L.E. Chirkov, Physical Principles of Acousto-Optics, Radio i Szyaz, Moscow, 1985.
[5] P.D. Das, C.M. DeCusatis, Acousto-Optic Signal Processing: Fundamentals & Applications, Artech House, Boston, 1991.
[6] R.W. Klein, B.D. Cook, A unified approach to ultrasonic light diffraction, IEEE Transactions SU-14 (3) (1967) 123–134.
[7] V.G. Dmitriev, G.G. Gurzadyan, D.N. Nikogosyan, Handbook of Nonlinear Optical Crystals, third ed., Springer, Berlin, 1999.
[8] K. Dodd, J.C. Eilbeck, J.D. Gibbon, H. Morris, Solitons and Nonlinear Wave Equations, Academic Press, Orlando, 1984.